CrossMark

electronic reprint

Acta Crystallographica Section B
Structural Science, Crystal Engineering and Materials
ISSN 2052-5206

First experimental charge density study using a Bruker CMOS-type PHOTON 100 detector: the case of ammonium tetraoxalate dihydrate

Katarzyna N. Jarzembska, Radosław Kamiński, Łukasz Dobrzycki and Michał K. Cyrański

Acta Cryst. (2014). B**70**, 847–855

Copyright © International Union of Crystallography

Author(s) of this paper may load this reprint on their own web site or institutional repository provided that this cover page is retained. Republication of this article or its storage in electronic databases other than as specified above is not permitted without prior permission in writing from the IUCr.

For further information see http://journals.iucr.org/services/authorrights.html

Acta Crystallographica Section B: Structural Science, Crystal Engineering and Materials publishes scientific articles related to the structural science of compounds and materials in the widest sense. Knowledge of the arrangements of atoms, including their temporal variations and dependencies on temperature and pressure, is often the key to understanding physical and chemical phenomena and is crucial for the design of new materials and supramolecular devices. *Acta Crystallographica B* is the forum for the publication of such contributions. Scientific developments based on experimental studies as well as those based on theoretical approaches, including crystal-structure prediction, structure–property relations and the use of databases of crystal structures, are published.

Crystallography Journals Online is available from **journals.iucr.org**

Acta Crystallographica Section B
Structural Science, Crystal Engineering and Materials
ISSN 2052-5206

First experimental charge density study using a Bruker CMOS-type PHOTON 100 detector: the case of ammonium tetraoxalate dihydrate

Katarzyna N. Jarzembska,[a,b]* Radosław Kamiński,[b] Łukasz Dobrzycki[a]* and Michał K. Cyrański[a]

[a]Czochralski Laboratory of Advanced Crystal Engineering, Biological and Chemical Research Centre, Department of Chemistry, University of Warsaw, Żwirki i Wigury 101, 02-089 Warsaw, Poland, and [b]Department of Chemistry, University at Buffalo, The State University of New York, Buffalo, NY 14260-3000, USA

Correspondence e-mail: katarzyna.jarzembska@gmail.com, dobrzyc@chem.uw.edu.pl

Received 14 April 2014
Accepted 30 July 2014

The aim of this study was to test the applicability of a Bruker AXS CMOS-type PHOTON 100 detector for the purpose of a fine charge density quality data collection. A complex crystal containing oxalic acid, ammonium oxalate and two water molecules was chosen as a test case. The data was collected up to a resolution of 1.31 Å^{-1} with high completeness (89.1%; $R_{\rm mrg}$ = 0.0274). The multipolar refinement and subsequent quantum theory of atoms in molecules (QTAIM) analysis resulted in a comprehensive description of the charge density distribution in the crystal studied. The residual density maps are flat and almost featureless. It was possible to derive reliable information on intermolecular interactions to model the anharmonic motion of a water molecule, and also to observe the fine details of the charge density distribution, such as polarization on O and H atoms involved in the strongest hydrogen bonds. When compared with our previous statistical study on oxalic acid data collected with the aid of CCD cameras, the complementary metal-oxide semiconductor (CMOS) detector can certainly be classified as a promising alternative in advanced X-ray diffraction studies.

1. Introduction

The introduction of area detectors, including charge-coupled devices (CCDs) which are the most commonly used nowadays, constituted one of the factors allowing for fast and effective X-ray diffraction data collections. Modern CCD cameras are characterized by high spatial resolution (small pixel size and large pixel number), low intrinsic noise and short read-out time when compared with the previously used point detectors (PDs; Yagi *et al.*, 2004; Dauter, 2006). Although the very first experimental charge density studies were performed with PDs (Coppens *et al.*, 1984; Ohba *et al.*, 1983; Hansen & Coppens, 1978; Stevens & Coppens, 1980; Ito & Sakurai, 1973; Almlöf *et al.*, 1973), which are still considered to be the most useful detectors for the very precise determination of unit cell constants (Schmidbauer *et al.*, 2012), PDs are not suitable for recording data for difficult cases, such as non-merohedrally twinned crystals (Parsons, 2003; Colombo *et al.*, 2000), analyses of modulated structures (Duisenberg *et al.*, 2003; Porta *et al.*, 2011) or diffuse-scattering-related phenomena (Osborn & Welberry, 1990). In addition, measurements of highly redundant charge density data with PDs are very time-consuming (*e.g.* 1–2 months; Flensburg *et al.*, 1995; Madsen *et al.*, 1998). On the other hand, Martin & Pinkerton (1998) showed that CCD cameras can be successfully used for high-resolution data collections leading to the determination of very high quality electron density distributions (Kuntzinger *et al.*, 1999; Macchi *et al.*, 1998; Graafsma *et al.*, 1997; Sørensen &

© 2014 International Union of Crystallography

electronic reprint

Table 1
Parameters characterizing the X-ray data collection and refinement.

Crystal data	
Chemical formula	$C_2H_2O_4{\cdot}C_2HO_4^-{\cdot}NH_4^+{\cdot}2H_2O$
M_r	233.14
Crystal system, space group	Triclinic, $P\bar{1}$
Temperature (K)	100
a, b, c (Å)	6.2372 (4), 7.1935 (5), 10.4745 (7)
α, β, γ (°)	94.5207 (18), 99.8882 (18), 96.7177 (19)
V (Å^3)	457.45 (5)
Z	2
$F(000)$	244
D_x (Mg m^{-3})	1.693
Radiation type	Mo $K\alpha$
θ values (°)	2.87–62.67
μ (mm^{-1})	0.174
Crystal colour and shape	Colourless block
Crystal size (mm)	0.24 × 0.21 × 0.09
Data collection	
Diffractometer	Bruker AXS B8 VENTURE
Absorption correction	Multi-scan (Blessing,1995)
T_{min}, T_{max}	0.966, 0.985
No. of measured and independent reflections	50 285, 14 225
R_{mrg}†	0.0273
$(\sin\theta/\lambda)_{max}$ (Å^{-1})	1.25‡
Range of h, k, l	$h = -15 \rightarrow 15$, $k = -17 \rightarrow 17$, $l = -26 \rightarrow 26$
Refinement	
No. of observed [$I \geq 3\sigma(I)$] reflections	9995 (70%)§
No. of parameters	349
No. of restraints	11
$R[F]$ [$I \geq 3\sigma(I)$], all data	0.0181, 0.0353
$wR[F]$ [$I \geq 3\sigma(I)$], all data	0.0190, 0.0226
$R[F^2]$ [$I \geq 3\sigma(I)$], all data	0.0295, 0.0316
$S[F]$ [$I \geq 3\sigma(I)$], all data	0.891, 0.885
H-atom treatment	H atoms treated by a mixture of restrained and constrained refinement
$\Delta\rho_{max}$, $\Delta\rho_{min}$ [$I \geq 3\sigma(I)$] (e Å^{-3})	0.21, −0.22
$\Delta\rho_{max}$, $\Delta\rho_{min}$ (all data) (e Å^{-3})	0.35, −0.34

† Definitions of R factors are summarized in the supporting information. ‡ All values given in this table are up to this resolution limit. § Completeness for observed reflections.

Larsen, 2003; Koritsánszky *et al.*, 1998; Coppens *et al.*, 1999), which displaced PDs in research laboratories.

Nevertheless, CCD detectors have some serious drawbacks. The most significant of these are definitely a limited dynamic range, relatively easy oversaturation, and a rather long readout time as for the current high-end experimental requirements. Therefore, new types of detectors are being designed, among which the most promising ones are based on complementary metal-oxide semiconductor (CMOS) technology. The CMOS detectors are said to be sensitive, low-noise and high-speed devices with wide dynamic range, high resolution and other advantages. It is also worth mentioning that modern so-called hybrid pixel array detectors, such as PILATUS (Broennimann *et al.*, 2006) or XPAD (Basolo *et al.*, 2005), are also partially based on the CMOS technology. However, the first detectors of this type have only recently been commercially introduced and their performance in different research areas is still being tested.

Hence, the aim of this short contribution is to verify the applicability of a Bruker AXS CMOS-type PHOTON 100 detector for the purpose of fine charge density quality data collection. As a test case we have chosen a complex crystal containing neutral molecules of oxalic acid and water, as well as ionic moieties of ammonium oxalate salt. This crystal is a perfect subject for our investigations, as it contains oxalic acid species explored in our recent statistical study of charge density data collected on a CCD detector (Kamiński *et al.*, 2014), but it also covers a greater variety of interactions and other subtle effects in the crystal lattice. In the current study we employed the multipole formalism (Hansen & Coppens, 1978) for charge density distribution modelling, whereas the obtained model was analysed with the aid of quantum theory of atoms in molecules (QTAIM; Bader, 1994).

2. Experimental

2.1. Crystallization, data collection and processing

A charge density quality single crystal of the title compound was grown from the saturated water solution by slow evaporation at room temperature. High-resolution single-crystal X-ray measurement of an ammonium tetraoxalate dihydrate crystal was carried out at 100 K on a Bruker AXS D8 VENTURE single-crystal diffractometer equipped with a CMOS-type PHOTON 100 area detector, molybdenum sealed X-ray tube (Mo $K\alpha$ radiation, λ = 0.71073 Å), four-circle goniometer, TRIUMPH monochromator, and an Oxford Cryosystems low-temperature nitrogen gas-flow device (Cryostream Plus). The 16 800 doubly correlated frames were collected utilizing the ω-scan mode according to the following strategy (thin rotation increment: $\Delta\omega$ = 0.25°; fixed Euler geometry parameters: χ = −56° and $\Delta\omega_{tot}$ = 150°):

(i) four scans with 2θ = −10° (φ = 0, 90, 180 and 270°) and 6 s of exposure time;

(ii) four scans with 2θ = −50° (φ = 0°, 90°, 180° and 270°) and 15 s of exposure time;

(iii) four scans with 2θ = 50° (φ = 0, 90, 180 and 270°) and 15 s of exposure time;

(iv) eight scans with 2θ = −100° (φ = 0, 45, 90, 135, 180, 225, 270 and 315°) and 40 s of exposure time;

(v) eight scans with 2θ = 100° (φ = 0, 45, 90, 135, 180, 225, 270 and 315°) and 40 s of exposure time.

The determination of unit-cell parameters and the integration of raw diffraction images were performed with the *APEX2* program package (Bruker, 2012). The data set was corrected for Lorentz, polarization and oblique incidence effects. The multi-scan absorption correction, frame-to-frame scaling and merging of reflections were carried out with the *SORTAV* program (Blessing, 1987, 1995, 1997). The data set is characterized by the high resolution of $(\sin\theta/\lambda)_{max}$ = 1.31 Å^{-1} and good overall completeness (89.1%; relative mean absolute

electronic reprint

deviation of the measurements: R_{mrg} = 0.0274; for a definition of R_{mrg} see the supporting information[1]). The final charge density model was based on the data up to the 1.25 Å^{-1} resolution limit (95.0%; R_{mrg} = 0.0273). It should be noted here that the 001 reflection was shaded by the beamstop. Its absence may lead to the deviation observed in the low-angle region of binned $|F_o|/|F_c|$ values plotted *versus* $\sin\theta/\lambda$ after the final refinement (supporting information, Fig. 4S). The final data collection and reduction parameters are presented in Table 1 and the supporting information.

2.2. Structure solution and refinement

Crystal structure was solved by a charge-flipping method (Oszlányi & Sütő, 2004, 2005; Palatinus, 2013) with the *SUPERFLIP* program (Palatinus & Chapuis, 2007). Initial independent atom model (IAM) refinements were performed with the *JANA* program (Petříček *et al.*, 2014).

Multipole refinement was conducted in the *MOPRO* suite (Jelsch *et al.*, 2005; Guillot *et al.*, 2001) combined with the current version of the University at Buffalo Data Bank (UBDB; Jarzembska & Dominiak, 2012), which employs the Hansen–Coppens multipole model (Hansen & Coppens, 1978). Refinement was based on F, and only the reflections fulfilling the $I \geq 3\sigma(I)$ condition were taken into account. Such a cut-off does not significantly influence the final model, as shown quite recently (results obtained with and without cut-off are within the method precision; Kamiński *et al.*, 2014). The statistical weights were used (*i.e.* for the ith reflection $w_i = 1/\sigma_i^2$). Initial atomic coordinates (x, y, z) and anisotropic displacement parameters (U^{ij}s) for each atom were taken from the independent-atom-model-based refinement, whereas initial multipolar and contraction–expansion parameters were transferred from UBDB with the aid of the *LSDB* program (Volkov *et al.*, 2004; Jarzembska & Dominiak, 2012). Additionally, the X—H bond lengths (X = non-H atom) were standardized to neutron-normalized distances according to the values tabulated by Allen & Bruno [d_{O-H} = 1.018 and 0.958 Å (water molecule), d_{N-H} = 1.035 Å; Allen *et al.*, 1987; Allen & Bruno, 2010]. The *MOPRO* program allows for the application of specific restraints during the refinement. Therefore, in the initial stage, the H-atom U_{iso} parameters (*i.e.* isotropic displacement parameters) were restrained to the value of $1.5U_{eq}$ with σ = 0.01 Å^2 (where an appropriate restraint weight is equal to $1/\sigma^2$). In the final stage of the refinement, the estimation of anisotropic H-atom atomic displacement parameters was realised using the *SHADE* server (Madsen, 2006; Munshi *et al.*, 2008). Due to the limitations of the rigid body model fit within the translation–libration–screw (TLS) formalism (Schomaker & Trueblood, 1968, 1998; Cruickshank, 1956; Sands, 1982), the H-atom atomic displacement parameters were obtained through a separate riding model approximation for each moiety. The X—H bond lengths were restrained to neutron-normalized distances with σ = 0.001 Å. This approach has recently been successfully tested in a variety of studies, providing results comparable with the corresponding theoretical periodic computations and neutron studies (Kamiński *et al.*, 2014; Jarzembska, Goral, *et al.*, 2013; Jarzembska *et al.*, 2012). All κ' parameters were kept fixed at the UBDB transferred values. The multipole expansion was truncated at the octupole (l_{max} = 3) and quadrupole (l_{max} = 2) levels for all non-H and H atoms, respectively. All atomic deformation density functions were subjected to the local symmetry constraints, suggested by the *LSDB* program (except for the NH_4^+ cation for which $\bar{4}3m$ point-group symmetry was manually assigned). In the case of H atoms solely the bond-directed dipole and quadrupole populations (*i.e.* P_{10} and P_{20}) were refined. The importance of proper treatment of local symmetry constraints and restraints in charge density studies has already been emphasized in a set of research papers (Poulain-Paul *et al.*, 2012; Zarychta *et al.*, 2011; Paul *et al.*, 2011).

Additionally it was found that the water O10 atom undergoes noticeable anharmonic motion. This behaviour has been successfully modelled using third-order Gram–Charlier parameters (Kuhs, 1983; Scheringer, 1985; Johnson, 1969), whereas the physical reliability of the anharmonic model was confirmed by the probability density function (PDF) computed with the *JANA* program. Additionally, the refined anharmonic parameters appeared to be rather weakly correlated with multipolar parameters (the average correlation coefficient was equal to $\sim$ 0.5, the maximal was equal to 0.79 for the C_{111} and Z -oriented dipole). These results are among many recent literature reports on this matter (Poulain *et al.*, 2014; Herbst-Irmer *et al.*, 2013; Zhurov *et al.*, 2011; Scheins *et al.*, 2010), where high-quality data allow for clear deconvolution of electron density and thermal motion features.

The general strategy for the refinement was as follows:

(i) scale factor (which was also refined in almost all other stages);

(ii) atomic coordinates;

(iii) atomic coordinates and atomic displacement parameters;

(iv) *SHADE* estimation of anisotropic H-atom atomic displacement parameters (which was also updated in-between other stages until convergence);

(v) multipole population parameters in a stepwise manner;

(vi) all multipole population parameters and structural parameters simultaneously;

(vii) block refinement of non-H atom κ parameters (first block), step No. (vi) (second block), and the third-order anharmonic parameters for the O10 atom [no scale factor refined; $(\sin\theta/\lambda) \geq 0.8$ Å^{-1}] (third block);

(viii) all parameters simultaneously.

The final model is characterized by flat and close-to-featureless residual density distribution. Residual density properties were evaluated with the *JNK2RDA* program (Meindl & Henn, 2008). The Hirshfeld rigid-bond test (Hirshfeld, 1976) was well fulfilled for all bonds between non-H atoms. All final refinement statistics are summarized in Table 1. The corresponding CIF file is present in the supporting information.

[1] Supporting information for this paper is available from the IUCr electronic archives (Reference: PI5019).

electronic reprint

Table 2
Distribution of measured reflections in equal-volume resolution shells as taken from the *SORTAV* program.

$s_{max} = (\sin\theta/\lambda)_{max}$ – maximal resolution for a given shell; N_{shell} – number of measured reflections in a given shell; N – average redundancy in a given shell; R_{mrg} and R_{rms} – R factors corrected for small-sample measurement multiplicity as defined in the supporting information; C – data completeness.

s_{max} (Å^{-1})	N_{shell}	N	$I/\sigma(I)$	R_{mrg}	R_{rms}	C (%)
0.48	859	6.0	34.45	0.0246	0.0678	99.9
0.61	871	4.3	22.64	0.0258	0.0253	99.8
0.70	856	2.9	18.43	0.0350	0.0369	99.5
0.77	868	2.8	16.18	0.0376	0.0336	99.2
0.83	873	3.7	16.53	0.0420	0.0353	99.4
0.88	846	4.7	17.86	0.0426	0.0380	99.2
0.93	881	4.3	15.42	0.0508	0.0432	98.7
0.97	832	4.3	14.73	0.0535	0.0435	98.9
1.01	872	3.7	12.98	0.0618	0.0515	98.4
1.04	820	2.6	10.52	0.0640	0.0519	96.7
1.08	868	2.6	9.53	0.0765	0.0601	97.1
1.11	675	2.3	8.43	0.0836	0.0640	80.8
1.14	752	2.3	8.19	0.0825	0.0637	85.1
1.17	798	2.6	7.65	0.0951	0.0738	90.7
1.19	780	2.7	7.76	0.0948	0.0750	91.0
1.22	813	2.8	7.56	0.0995	0.0771	92.3
1.24	768	2.5	6.35	0.1155	0.0913	90.8
1.27	718	2.2	5.94	0.1182	0.0904	81.5
1.29	488	1.5	5.22	0.1241	0.0920	57.0
1.31	859	6.0	3.92	0.0246	0.0678	26.5

2.3. Evaluation of the experimental charge density distribution properties

The experimental charge density distribution obtained with the multipolar approach was analysed by means of Bader's quantum theory of atoms in molecules (QTAIM; Bader, 1994). The *VMOPRO* module (part of the *MOPRO* package) was used for Fourier syntheses and bond critical point (BCP) evaluation. Visualization of bond paths was accomplished with the *MOPROVIEWER* program (Guillot, 2012). The neighbouring molecules selected for the bond path search were prepared using the *CLUSTERGEN* program (Kamiński *et al.*, 2013). Evaluation and integration of atomic basins were performed with the *WINXPRO* program (Stash & Tsirelson, 2002, 2005).

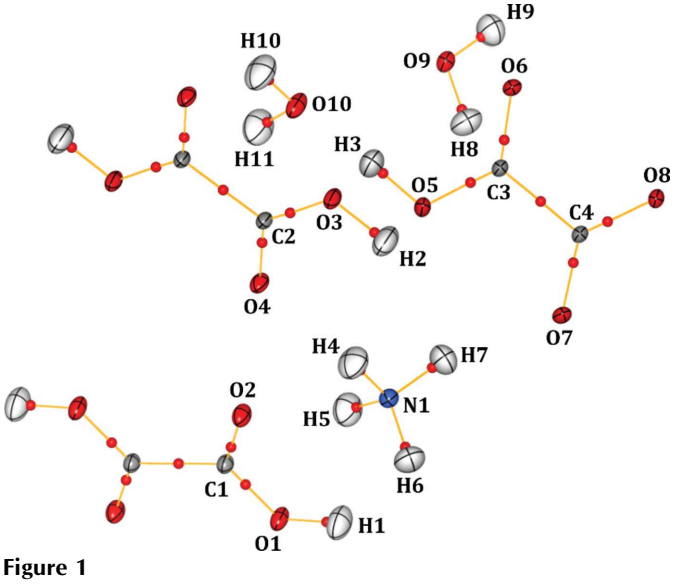

Figure 1
Molecular graph showing bond paths (golden solid lines) and bond critical points (small red spheres) for the crystal structure studied. Labelling (only ASU) and estimation of atomic displacement parameters is included (ellipsoids are drawn at the 50% probability level).

3. Crystal structure

The crystal structure chosen for the purpose of our studies, containing ammonium oxalate species, oxalic acid molecule and two water moieties, has already been the subject of several earlier investigations. The first report concerning room-temperature neutron diffraction studies was in the 1960s (Currie *et al.*, 1967) and the structure was redetermined in 2006, also at 298 K, using the single-crystal X-ray diffraction technique (Portalone & Colapietro, 2006).

As an oxalic acid molecule dissociates easily in a water environment, which is reflected by its low pK_a values (pK_{a1} = 1.27, pK_{a2} = 4.28; Morrison & Boyd, 1992), in the presence of a base reagent, such as ammonia vapour, it can be easily deprotonated yielding an ammonium oxalate salt, $[C_2HO_4^-][NH_4^+]$. Furthermore, even a vestigial amount of ammonia in contact with a crystallization solution can be effectively absorbed and incorporated in the growing crystals. Under such conditions a complex crystal form can be obtained composed not only of ammonium oxalate, but, as mentioned before, also containing oxalic acid and two water molecules in the asymmetric unit ($[C_2H_2O_4][C_2HO_4^-][NH_4^+]\cdot 2H_2O$). The crystal can be described with the triclinic $P\bar{1}$ space group and the unit-cell parameters are almost identical with the previously reported values, taking into account differences in the measurement temperatures (Table 2). Since the crystal structure has already been analysed in detail in other contributions (Portalone & Colapietro, 2006; Currie *et al.*, 1967), here we just remark that in the asymmetric part of the unit cell (ASU) there are two symmetry-independent oxalic acid half molecules (Fig. 1). These molecular fragments form the whole molecules through the C1—C1^{i} or C2—C2^{ii} bonds, respectively [symmetry codes: (i) $-x+2, -y+2, -z+1$; (ii) $-x, -y+1, -z+1$].

4. Charge density data quality

First it should be noted that even using a sealed X-ray tube instead of a more powerful microfocus source or rotating anode, it was possible to collect high-quality X-ray diffraction data up to the impressive resolution of $(\sin\theta/\lambda)_{max}$ = 1.31 Å^{-1} with high overall completeness (89.1%; R_{mrg} = 0.0274), in a reasonable time of ~175 h (*ca* 1 week). This may indeed confirm the advertised high sensitivity of the PHOTON 100 detector. Additionally, the data is characterized by good statistics when processed with the *APEX2* software (Bruker, 2012) and later with the *SORTAV* (Blessing, 1987, 1995, 1997) program (Table 2). Nevertheless, the very high-resolution part of the data lacks completeness, which is 26.5% at worst. Thus, for the purpose of further refinement, the resolution was cut down to 1.25 Å^{-1} (95.0%, R_{mrg} = 0.0273), which remains high-

electronic reprint

end as for a charge density study of an organic crystal. The lowest-resolution data is almost fully complete (only the 001 reflection was shaded by the beamstop), and thus the overall statistics compare well to other high-quality charge density studies performed using a rotating anode X-ray source (Zhurov *et al.*, 2005).

The data quality and the adequacy of the fitted model is supported by quite featureless residual density maps (Figs. 2*a* and *b*) with the residues not larger than about ±0.22 and ±0.35 e Å^{-3} for statistically significant [$I \geq 3\sigma(I)$] and all reflections, respectively. Nevertheless, it should be noted that some of the residual density peaks are present along the bonds. These are, however, comparable in height to some other more randomly located peaks, and are more pronounced when weak reflections [$I \ll 3\sigma(I)$] are used in the Fourier summation. Such an effect might be attributed to the insufficient CMOS detector corrections, which are known to be non-linear (Kaercher *et al.*, 2011). Since differently parametrized models do not remove these features, they are most likely caused by some deficiencies in the raw data processing.

The residual density fractal plots shown in Fig. 3 indicate an even distribution of residual maxima and minima, which does not change much qualitatively when all data is taken into account. Nevertheless, it should be noted that the fractal dimension value does not significantly exceed 2.5, despite the high resolution of the examined data set. This might be the reason for the apparently higher noise level than that observed for typical CCD detectors (Skarzynski, 2013).

Table 3
The final third-order Gram–Charlier (GC) parameters for the O10 atom.

The most significant values are shown in bold.

GC parameter	Refined value	GC parameter	Refined value
C_{111}	−0.0002 (1)	C_{113}	0.0001 (1)
C_{222}	**0.00171 (7)**	C_{133}	−0.00028 (6)
C_{333}	0.00009 (3)	C_{223}	**0.0022 (1)**
C_{112}	0.0006 (1)	C_{233}	0.00093 (5)
C_{122}	**−0.0018 (1)**	C_{123}	**−0.0015 (1)**

High-resolution X-ray data of sufficient quality is indispensable for a proper deconvolution of static charge density features and atomic thermal motion (Henn *et al.*, 2010; Iversen *et al.*, 1999). In the case of our measurement, it was relatively easily achievable within the model limits. What is more, it was possible to detect and model the observed anharmonic motion at the O10 atom belonging to one of the water species. As illustrated in Fig. 4(*a*), before the modelling a characteristic alternated residual density pattern (Herbst-Irmer *et al.*, 2013; Poulain *et al.*, 2014) at high-order data is clearly seen. Using only the third-order Gram–Charlier (GC) expansion parameters (Table 3), the anharmonic motion of the O atom was successfully modelled (Fig. 4*b*), leading to a clear residual density map. It is worth noting that some of the GC parameters (*e.g.* C_{111} or C_{223}) are very significant, indicating the strength of the observed anharmonic signal (due to the very high resolution of the data set).

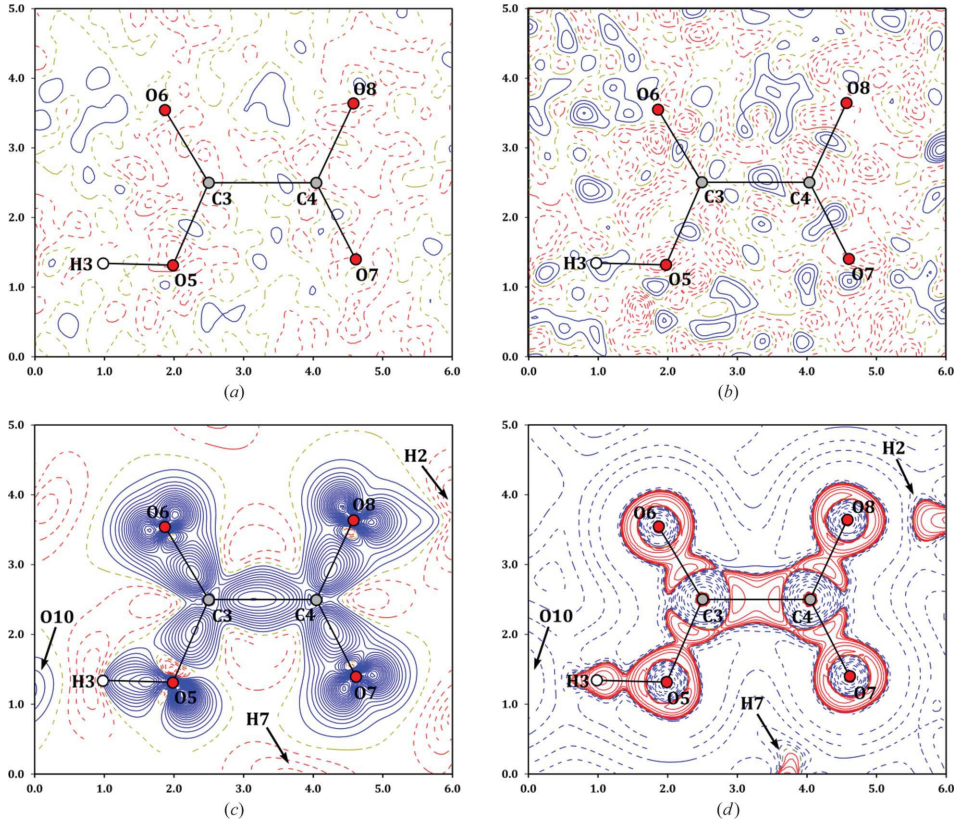

Figure 2
(*a*), (*b*) Residual density maps for the $C_2HO_4^-$ anion calculated either for reflections with $I \geq 3\sigma(I)$ (*a*), or for all reflections (*b*). (*c*), (*d*) Deformation density (*c*) and negative Laplacian (*d*) maps for the same molecular fragment. Contours and colour coding: (*a*), (*b*), (*c*) linear 0.05 e Å^{-3} contours; blue solid lines – positive values, red dashed lines – negative values; (*d*) logarithmic contours; red solid lines – positive values, blue dashed lines – negative values.

5. Evaluation and analysis of charge density distribution properties

The sensibility of the derived charge density distribution can be judged on the basis of its features and related properties, such as atomic charges *etc.* These in turn reflect to a great extent the quality of the collected data, especially in the case of organic systems, the charge density distribution of which can be well reproduced using the multipolar formalism of Hansen & Coppens (1978).

For the purpose of our study, the obtained charge density distribution was explored with the QTAIM approach. The analysis resulted in a

electronic reprint

complete picture of bond paths (BPs) and bond critical points (BCPs) within the molecular fragments illustrated in Fig. 1, together with a set of reasonable atomic and summary molecular fragment charges given in Table 4. As expected, the two oxalic acid molecules, reconstructed using an appropriate symmetry operation, can be considered as neutral within the method accuracy, similar to two water moieties. On the other hand, the oxalate anion is characterized by significant negative charge close to −1, whereas the ammonium cation has almost exactly the opposite charge of *ca* +1. Interestingly, the fragment volumes of the two symmetry-independent oxalic acid molecules are different, and one of them seems to be very similar to the oxalate anion. On the other hand, two water molecules are spatially very similar, although the second one (O10, H10, H11) seems to be slightly larger in volume (*ca* 1 Å^3). Additionally, the O10 atom, having a bit more space around itself, can undergo a detectable anharmonic motion and in this respect the QTAIM analysis is consistent with the earlier observed phenomenon. This is again the result of intermolecular forces and a specific set of strong hydrogen-bonded interactions dominating the structure.

The analysis of atomic charges unveils the same chemically plausible picture of the crystal. O atoms are the most negatively charged species, whereas the C atoms exhibit large positive charges. There is a visible charge difference between the C3 and C4 atoms which is in agreement with the chemical intuition. The deprotonated part of the anion (C4, O7 and O8 atoms), where supposedly the negative charge is localized, is characterized by the above-mentioned C4 atom being more positively charged than C3 (and accordingly smaller than C3), and also with the O7 and O8 atoms which are slightly more negative when compared with the other two O atoms on the other side of the oxalate fragment.

A closer look at the property values evaluated at BCPs (Table 5) confirms further the reliability of the refined electron density distribution model. Whereas the oxalic acid molecule properties are very similar to those previously studied (Kamiński *et al.*, 2014), except for the above-mentioned molecular volume of the second oxalic acid moiety, the oxalate anion is noticeably different. The electron density and its

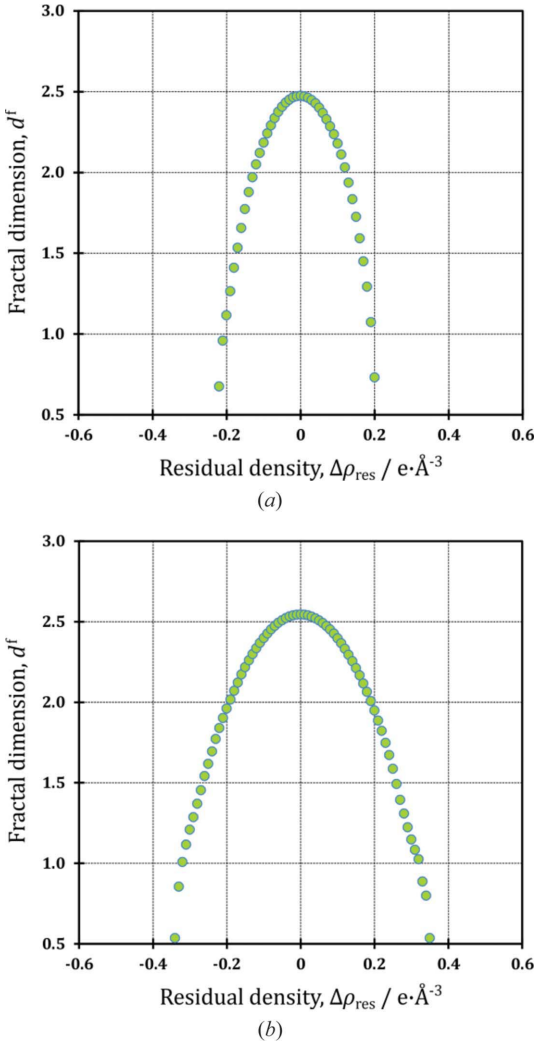

Figure 3
Residual density fractal plots: (*a*) for reflections fulfilling the $I \geq 3\sigma(I)$ condition; (*b*) for all reflections.

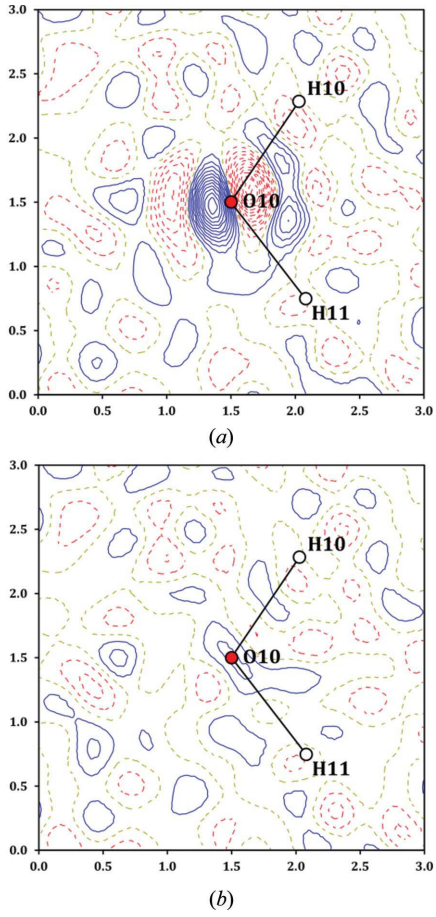

Figure 4
High-resolution [$(\sin\theta/\lambda) \geq 0.8$ Å^{-1}] residual density maps for a second water molecule before (*a*) and after (*b*) modelling of the anharmonicity features with third-order Gram–Charlier parameters. Maps computed with reflections fulfilling the $I \geq 3\sigma(I)$ condition; linear 0.03 e Å^{-3} contours; blue solid lines – positive values, red dashed lines – negative values.)

electronic reprint

Table 4
Atomic (Q_i, V_i) and fragment ($\sum_i Q_i$, $\sum_i V_i$) Bader charges for the crystal in the crystal lattice.

Atom	Q_i (e)	V_i (Å^3)
C1	+1.54	4.52
O1	−1.04	15.33
O2	−1.16	17.25
H1	+0.66	1.05
C2	+1.54	5.38
O3	−1.06	16.59
O4	−1.16	16.64
H2	+0.67	1.05
C3	+1.49	5.14
C4	+1.57	4.87
O5	−1.11	16.91
O6	−1.18	17.38
O7	−1.23	16.45
O8	−1.13	17.22
H3	+0.66	1.14
N1	−1.73	18.43
H4	+0.68	1.70
H5	+0.67	1.67
H6	+0.65	1.80
H7	+0.64	1.66
O9	−1.26	19.13
H8	+0.66	1.57
H9	+0.64	1.69
O10	−1.23	19.67
H10	+0.62	1.76
H11	+0.61	1.91

Fragment	$\sum_i Q_i$ (e)	$\sum_i V_i$ (Å^3)
$C_2H_2O_4$ (first)†	+0.01	76.28
$C_2H_2O_4$ (second)‡	−0.02	79.32
$C_2HO_4^-$	−0.93	79.11
NH_4^+	+0.91	25.26
H_2O (first)§	+0.04	22.40
H_2O (second)¶	+0.00	23.34

† Oxalic acid molecule: 2 × (C1, O1, O2, H1). ‡ Oxalic acid molecule: 2 × (C2, O3, O4, H2). § Water molecule: O9, H8, H9. ¶ Water molecule: O10, H10, H11.

Table 5
Selected QTAIM parameters of strong intramolecular interactions at BCPs detected in the studied crystal structure.

d – distance between bonded atoms; d_1 and d_2 – distances from the first and second atom to the BCP, respectively; ϱ — electron density; ϵ – bond ellipticity.

Fragment	Bond	d (Å)	d_1 (Å)	d_2 (Å)	$\varrho(\mathbf{r}_{BCP})$ (e Å^{-3})	$\nabla^2\varrho(\mathbf{r}_{BCP})$ (e Å^{-5})	ε
$C_2H_2O_4$ (first)†	C1—O1	1.2879 (3)	0.480	0.808	2.48	−27.4	0.09
	C1—O2	1.2238 (3)	0.428	0.796	2.91	−27.1	0.10
	C1—C1^{i}	1.5398 (2)	0.770	0.770	1.73	−13.4	0.17
	O1—H1	1.018 (1)	0.800	0.218	1.92	−43.4	0.00
$C_2H_2O_4$ (second)‡	C2—O3	1.2860 (3)	0.483	0.803	2.47	−27.9	0.11
	C2—O4	1.2266 (3)	0.434	0.793	2.91	−30.6	0.12
	C2—C2^{ii}	1.5490 (1)	0.775	0.775	1.72	−13.4	0.22
	O3—H2	1.018 (1)	0.808	0.210	1.90	−47.1	0.00
$C_2HO_4^-$	C3—C4	1.5507 (2)	0.786	0.764	1.68	−12.0	0.21
	C3—O5	1.2970 (3)	0.490	0.807	2.44	−26.7	0.09
	C3—O6	1.2217 (3)	0.428	0.794	2.90	−26.9	0.11
	C4—O7	1.2428 (3)	0.437	0.806	2.74	−25.9	0.06
	C4—O8	1.2608 (3)	0.456	0.805	2.67	−29.2	0.08
	O5—H3	1.018 (1)	0.790	0.228	2.05	−43.8	0.00
NH_4^+	N1—H4	1.036 (1)	0.829	0.207	2.00	−43.8	0.00
	N1—H5	1.036 (1)	0.830	0.206	1.97	−42.6	0.00
	N1—H6	1.036 (1)	0.823	0.213	2.00	−41.2	0.00
	N1—H7	1.036 (1)	0.823	0.213	2.06	−44.2	0.00
H_2O (first)§	O9—H8	0.958 (1)	0.754	0.204	2.44	−62.6	0.00
	O9—H9	0.958 (1)	0.754	0.204	2.47	−64.3	0.00
H_2O (second)¶	O10—H10	0.958 (1)	0.738	0.220	2.59	−61.7	0.01
	O10—H11	0.958 (1)	0.739	0.219	2.59	−63.1	0.01

Symmetry codes: (i) $-x+2, -y+2, -z+1$; (ii) $-x, -y+1, -z+1$. † Oxalic acid molecule: 2 × (C1, O1, O2, H1). ‡ Oxalic acid molecule: 2 × (C2, O3, O4, H2). § Water molecule: O9, H8, H9. ¶ Water molecule: O10, H10, H11.

Laplacian values are lower for the C3—C4 bond when compared with the C1—C1^{i} and C2—C2^{ii} bonds. In addition, the observed ellipticity values for C4—O7 and C4—O8 are slightly smaller than these describing the two remaining carbon—oxygen bonds. Nevertheless, even though such fine differences are observed and the moieties seem to be distinguishable, one should always consider the overall method precision.

So as to complement the picture of the studied crystal in terms of charge density distribution properties, we have also detected and characterized intermolecular interactions. Numerical data is summarized in Table 6. As expected, the crystal network is rich in strong electrostatic interactions, including an extensive net of hydrogen bonds. In addition, the presence of charged species enhances the interaction strengths between some molecular fragments. The two strongest hydrogen bonds are formed between the first oxalic acid molecule and the first water molecule, and the second oxalic acid molecule and oxalate anion. These two interactions are characterized by short interatomic distances (< 1.47 Å) and very large electron density (> 0.7 e Å^{-3}) and negative Laplacian (< 2.5 e Å^{-5}) values at their BCPs. This clearly indicates the covalent character of these interatomic contacts. It is worth noting that the e.s.d. of the Laplacian for such strong hydrogen bonds can reach values up to 1 e Å^{-5} (Kamiński *et al.*, 2014), so the above conclusions are definitely sensible. The specific nature of these contacts is additionally emphasized by clear polarization of the O atoms, O8 and O9, visible in the deformation density maps (Fig. 2*c*, see supporting information). Furthermore, the contact between the oxalate anion and the second oxalic acid molecule was found to be particularly interesting. It appears that the H2 atom shifts towards the middle point between the two O atoms, *i.e.* O8 and O3, when refined freely. It might be then strongly shared between the two molecules, which can explain similar volumes of the two species and also subtle differences between the two neutral oxalic acid fragments found in the studied crystal structure. The third strong hydrogen bond (O10···H3) is also characterized by a short interatomic distance [1.479 (1) Å], but the BCP electron density is clearly smaller (0.57 e Å^{-3}) and the Laplacian is definitely positive (0.33 e Å^{-5}). This indicates the closed-shell interaction, although most probably with a significant covalent contribution when compared with a 'common' hydrogen bond.

All other observed hydrogen bonds are rather typical in nature and characterized with reasonable values of BCP electron density (< 0.3 e Å^{-3}) and positive Laplacian values.

electronic reprint

Table 6
A set of QTAIM parameters for selected weak intermolecular interactions at the positions of respective BCPs.

G – kinetic energy density; V – potential energy density.

Fragments involved	Weak interaction	d (Å)	d_1 (Å)	d_2 (Å)	$\varrho(\mathbf{r}_{BCP})$ (e Å^{-3})	$\nabla^2\varrho(\mathbf{r}_{BCP})$ (e Å^{-5})	$G(\mathbf{r}_{BCP})$ (kJ mol^{-1} a$_0^{-3}$)	$V(\mathbf{r}_{BCP})$ (kJ mol^{-1} a$_0^{-3}$)
$C_2H_2O_4$ (first)†···H_2O (first)‡	H1···O9^{i}	1.4392 (4)	0.465	0.974	0.79	−2.73	159.55	−393.42
$C_2H_2O_4$ (second)§···$C_2HO_4^-$	O8···H2^{ii}	1.4653 (4)	0.979	0.486	0.76	−2.69	148.06	−369.46
$C_2HO_4^-$···H_2O (second)¶	H3···O10^{iii}	1.479 (1)	0.457	1.023	0.57	0.33	130.21	−251.51
$C_2HO_4^-$···H_2O (first)§	O6···H9^{iv}	1.7823 (4)	1.148	0.636	0.28	1.46	63.17	−86.65
$C_2HO_4^-$···H_2O (first)‡	O7···H8^{v}	1.7586 (4)	1.162	0.598	0.26	1.65	62.59	−80.14
$C_2HO_4^-$···NH_4^+	H7···O7^{iii}	1.901 (2)	0.690	1.218	0.23	0.80	42.08	−62.31
$C_2H_2O_4$ (first)†···H_2O (second)¶	O2···H10^{vi}	1.8670 (5)	1.209	0.660	0.20	1.38	46.81	−55.98
$C^2H_2O_4$ (first)†···NH_4^+	O2···H5^{iii}	1.903 (2)	1.233	0.674	0.18	1.42	44.48	−50.30
$C_2H_2O_4$ (second)§···H_2O (second)¶	O4···H11^{vi}	1.9476 (6)	1.233	0.719	0.18	1.25	40.74	−47.57
$C_2H_2O_4$ (second)§···NH_4^+	H4···O4^{iii}	1.952 (2)	0.697	1.261	0.16	1.35	38.74	−40.57
$C_2HO_4^-$···NH_4^+	O6···H6^{vii}	1.9519 (6)	1.258	0.698	0.15	1.50	41.07	−41.35
$C_2H_2O_4$ (second)§···H_2O (second)¶	O3···H11^{viii}	2.275 (1)	1.380	0.899	0.07	1.13	24.71	−18.57

Symmetry codes: (i) $x, y+1, z$; (ii) $-x, -y+1, -z$; (iii) x, y, z; (iv) $-x+1, -y, -z$; (v) $-x+1, -y+1, -z$; (vi) $-x+1, -y+1, -z+1$; (vii) $x, y-1, z$; (viii) $x-1, y, z$. † Oxalic acid molecule: 2 × (C1, O1, O2, H1). ‡ Oxalic acid molecule: 2 × (C2, O3, O4, H2). § Water molecule: O9, H8, H9. ¶ Water molecule: O10, H10, H11.

However, a significant H-atom polarization visible on the Laplacian maps (Fig. 2*d*, see the supporting information) should be highlighted here. Such polarizations have already been reported in the literature (Śledź *et al.*, 2010; Jarzembska, Kamiński, *et al.*, 2013; Jarzembska, Goral *et al.*, 2013; Hoser *et al.*, 2010, 2012; Overgaard *et al.*, 2001; Roversi & Destro, 2004) and result from the refinement of quadrupole terms on H atoms. In our case, all bond-oriented dipole and quadrupole populations for H atoms are statistically significant. Also, these results together with our previous findings regarding oxalic acid (Kamiński *et al.*, 2014) provide a straightforward indication that such multipolar expansion components are important and cannot be neglected. The observed H-atom polarizations are in agreement with the nature of strong hydrogen bonds and further confirm the data quality. Interestingly, despite the refinement of dipole and quadrupole terms for all the H atoms, such polarizations are not observed for the N—H hydrogen atoms (see the supporting information), which is in accordance with the experimentally derived geometrical and topological features of the N—H···O contacts (Table 6).

6. Summary and conclusions

Our contribution constitutes the first in-house charge density study conducted using a Bruker AXS CMOS-type PHOTON 100 detector. The performed analyses confirm the quality of the collected data for a complex crystal containing oxalic acid, ammonium oxalate and two water molecules. Despite using a sealed tube as an X-ray source, the data was collected up to a resolution of 1.31 Å^{-1} with high completeness (89.1%; R_{mrg} = 0.0274), applying standard exposure times. This supports the high sensitivity of the employed CMOS detector. The multipolar refinement and subsequent QTAIM investigations resulted in a comprehensive and reliable description of the charge density distribution in the studied crystal and related properties. It was possible to derive sensible information on intermolecular interactions, to model the anharmonic motion of a water molecule, and observe a polarized charge density distribution on O and H atoms involved in the strongest hydrogen bonds.

Finally, in view of the above and also when compared with our previous statistical study on oxalic acid data collected with the aid of CCD cameras, it can be concluded that the CMOS-type PHOTON 100 detector can be classified as a *promising* alternative in the most demanding X-ray diffraction studies, such as charge density experiments. We believe that our research will stimulate further careful (re)examinations of CMOS area detector data-processing methods and comparative analyses on a wider range of crystals. All that will contribute to the improvement of the CMOS data treatment as well as encourage crystallographers to conduct more sophisticated research using this technology.

The X-ray measurement was performed in the Czochralski Laboratory of Advanced Crystal Engineering (Department of Chemistry, University of Warsaw) established by generous support from the Polish Ministry of Science and Higher Education (grant No. 614/FNiTP/115/2011). The research was supported by the National Science Centre (grant NCN 2011/03/B/ST4/02591). KNJ thanks the Polish Ministry of Science and Higher Education for financial support within the 'Mobility Plus' programme. Authors gratefully acknowledge Bruker AXS for cooperation, partnership and support, and Holger Ott (Karlsruhe, Germany) for his useful comments. Finally, we would like to thank Robert Blessing (Buffalo, NY, USA), Victor Young (Minneapolis, MN, USA), and both referees for their helpful comments.

References

Allen, F. H. & Bruno, I. J. (2010). *Acta Cryst.* B**66**, 380–386.
Allen, F. H., Kennard, O., Watson, D. G., Brammer, L., Orpen, A. G. & Taylor, R. (1987). *J. Chem. Soc. Perkin Trans. 2*, pp. S1–S19.
Almlöf, J., Kvick, Å. & Thomas, J. O. (1973). *J. Chem. Phys.* **59**, 3901–3906.
Bader, R. F. W. (1994). *Atoms in Molecules: A Quantum Theory*. Oxford University Press.

electronic reprint

Basolo, S., Berar, J., Boudet, N., Breugnon, P., Caillot, B., Clemens, J., Delpierre, P., Dinkespiler, B., Koudobine, I., Meessen, C., Menouni, M., Mouget, C., Pangaud, P., Potheau, R. & Vigeolas, E. (2005). *IEEE Trans. Nucl. Sci.* **52**, 1994–1998.

Blessing, R. H. (1987). *Cryst. Rev.* **1**, 3–58.

Blessing, R. H. (1995). *Acta Cryst.* A**51**, 33–38.

Blessing, R. H. (1997). *J. Appl. Cryst.* **30**, 421–426.

Broennimann, Ch., Eikenberry, E. F., Henrich, B., Horisberger, R., Huelsen, G., Pohl, E., Schmitt, B., Schulze-Briese, C., Suzuki, M., Tomizaki, T., Toyokawa, H. & Wagner, A. (2006). *J. Synchrotron Rad.* **13**, 120–130.

Bruker AXS (2012). *APEX2.* Bruker Instruments AXS, Madison, Wisconsin, USA.

Colombo, D. G., Young, V. G. & Gladfelter, W. L. (2000). *Inorg. Chem.* **39**, 4621–4624.

Coppens, P., Abramov, Y., Carducci, M., Korjov, B., Novozhilova, I., Alhambra, C. & Pressprich, M. R. (1999). *J. Am. Chem. Soc.* **121**, 2585–2593.

Coppens, P., Dam, J., Harkema, S., Feil, D., Feld, R., Lehmann, M. S., Goddard, R., Krüger, C., Hellner, E., Johansen, H., Larsen, F. K., Koetzle, T. F., McMullan, R. K., Maslen, E. N. & Stevens, E. D. (1984). *Acta Cryst.* A**40**, 184–195.

Cruickshank, D. W. J. (1956). *Acta Cryst.* **9**, 754–756.

Currie, M., Speakman, J. C. & Curry, N. A. (1967). *J. Chem. Soc. A*, pp. 1862–1869.

Dauter, Z. (2006). *Acta Cryst.* D**62**, 1–11.

Duisenberg, A. J. M., Kroon-Batenburg, L. M. J. & Schreurs, A. M. M. (2003). *J. Appl. Cryst.* **36**, 220–229.

Flensburg, C., Larsen, S. & Stewart, R. F. (1995). *J. Phys. Chem.* **99**, 10130–10141.

Graafsma, H., Svensson, S. O. & Kvick, Å. (1997). *J. Appl. Cryst.* **30**, 957–962.

Guillot, B. (2012). *Acta Cryst.* A**68**, s204.

Guillot, B., Viry, L., Guillot, R., Lecomte, C. & Jelsch, C. (2001). *J. Appl. Cryst.* **34**, 214–223.

Hansen, N. K. & Coppens, P. (1978). *Acta Cryst.* A**34**, 909–921.

Henn, J., Meindl, K., Oechsner, A., Schwab, G., Koritsanszky, T. & Stalke, D. (2010). *Angew. Chem. Int. Ed.* **49**, 2422–2426.

Herbst-Irmer, R., Henn, J., Holstein, J. J., Hübschle, C. B., Dittrich, B., Stern, D., Kratzert, D. & Stalke, D. (2013). *J. Phys. Chem. A*, **117**, 633–641.

Hirshfeld, F. L. (1976). *Acta Cryst.* A**32**, 239–244.

Hoser, A. A., Dobrzycki, Ł., Gutmann, M. J. & Woźniak, K. (2010). *Cryst. Growth Des.* **10**, 5092–5104.

Hoser, A. A., Jarzembska, K. N., Dobrzycki, Ł., Gutmann, M. J. & Woźniak, K. (2012). *Cryst. Growth Des.* **12**, 3526–3539.

Ito, T. & Sakurai, T. (1973). *Acta Cryst.* B**29**, 1594–1603.

Iversen, B. B., Larsen, F. K., Pinkerton, A. A., Martin, A., Darovsky, A. & Reynolds, P. A. (1999). *Acta Cryst.* B**55**, 363–374.

Jarzembska, K. N. & Dominiak, P. M. (2012). *Acta Cryst.* A**68**, 139–147.

Jarzembska, K. N., Goral, A. M., Gajda, R. & Dominiak, P. M. (2013). *Cryst. Growth Des.* **13**, 239–254.

Jarzembska, K. N., Kamiński, R., Wenger, E., Lecomte, C. & Dominiak, P. M. (2013). *J. Phys. Chem. C*, **117**, 7764–7775.

Jarzembska, K. N., Kubsik, M., Kamiński, R., Woźniak, K. & Dominiak, P. M. (2012). *Cryst. Growth Des.* **12**, 2508–2524.

Jelsch, C., Guillot, B., Lagoutte, A. & Lecomte, C. (2005). *J. Appl. Cryst.* **38**, 38–54.

Johnson, C. K. (1969). *Acta Cryst.* A**25**, 187–194.

Kaercher, J., Ruf, M., Durst, R. D. & Wachter, G. (2011). *Acta Cryst.* A**67**, C652.

Kamiński, R., Domagała, S., Jarzembska, K. N., Hoser, A. A., Sanjuan-Szklarz, W. F., Gutmann, M. J., Makal, A., Malińska, M., Bąk, J. M. & Woźniak, K. (2014). *Acta Cryst.* A**70**, 72–91.

Kamiński, R., Jarzembska, K. N. & Domagała, S. (2013). *J. Appl. Cryst.* **46**, 540–543.

Koritsanszky, T., Flaig, R., Zobel, D., Krane, H., Morgenroth, W. & Luger, P. (1998). *Science*, **279**, 356–358.

Kuhs, W. F. (1983). *Acta Cryst.* A**39**, 148–158.

Kuntzinger, S., Dahaoui, S., Ghermani, N. E., Lecomte, C. & Howard, J. A. K. (1999). *Acta Cryst.* B**55**, 867–881.

Macchi, P., Proserpio, D. M., Sironi, A., Soave, R. & Destro, R. (1998). *J. Appl. Cryst.* **31**, 583–588.

Madsen, A. Ø. (2006). *J. Appl. Cryst.* **39**, 757–758.

Madsen, D., Flensburg, C. & Larsen, S. (1998). *J. Phys. Chem. A*, **102**, 2177–2188.

Martin, A. & Pinkerton, A. A. (1998). *Acta Cryst.* B**54**, 471–477.

Meindl, K. & Henn, J. (2008). *Acta Cryst.* A**64**, 404–418.

Morrison, R. T. & Boyd, R. N. (1992). *Organic Chemistry.* New York: Prentice-Hall International.

Munshi, P., Madsen, A. Ø., Spackman, M. A., Larsen, S. & Destro, R. (2008). *Acta Cryst.* A**64**, 465–475.

Ohba, S., Sato, S., Saito, Y., Ohshima, K.-I. & Harada, J. (1983). *Acta Cryst.* B**39**, 49–53.

Osborn, J. C. & Welberry, T. R. (1990). *J. Appl. Cryst.* **23**, 476–484.

Oszlányi, G. & Sütő, A. (2004). *Acta Cryst.* A**60**, 134–141.

Oszlányi, G. & Sütő, A. (2005). *Acta Cryst.* A**61**, 147–152.

Overgaard, J., Schiøtt, B., Larsen, F. K. & Iversen, B. B. (2001). *Chem. Eur. J.* **7**, 3756–3767.

Palatinus, L. (2013). *Acta Cryst.* B**69**, 1–16.

Palatinus, L. & Chapuis, G. (2007). *J. Appl. Cryst.* **40**, 786–790.

Parsons, S. (2003). *Acta Cryst.* D**59**, 1995–2003.

Paul, A., Kubicki, M., Jelsch, C., Durand, P. & Lecomte, C. (2011). *Acta Cryst.* B**67**, 365–378.

Petříček, V., Dušek, M. & Palatinus, L. (2014). *Z. Kristallogr.* **229**, 345–352.

Porta, J., Lovelace, J. J., Schreurs, A. M. M., Kroon-Batenburg, L. M. J. & Borgstahl, G. E. O. (2011). *Acta Cryst.* D**67**, 628–638.

Portalone, G. & Colapietro, M. (2006). *Acta Cryst.* E**62**, o4725–o4727.

Poulain, A., Wenger, E., Durand, P., Jarzembska, K. N., Kamiński, R., Fertey, P., Kubicki, M. & Lecomte, C. (2014). *IUCrJ*, **1**, 110–118.

Poulain-Paul, A., Nassour, A., Jelsch, C., Guillot, B., Kubicki, M. & Lecomte, C. (2012). *Acta Cryst.* A**68**, 715–728.

Roversi, P. & Destro, R. (2004). *Chem. Phys. Lett.* **386**, 472–478.

Sands, D. E. (1982). *Vectors and Tensors in Crystallography.* Reading, MA: Addinson-Wesley Publishing Company.

Scheins, S., Zheng, S.-L., Benedict, J. B. & Coppens, P. (2010). *Acta Cryst.* B**66**, 366–372.

Scheringer, C. (1985). *Acta Cryst.* A**41**, 79–81.

Schmidbauer, M., Kwasniewski, A. & Schwarzkopf, J. (2012). *Acta Cryst.* B**68**, 8–14.

Schomaker, V. & Trueblood, K. N. (1968). *Acta Cryst.* B**24**, 63–76.

Schomaker, V. & Trueblood, K. N. (1998). *Acta Cryst.* B**54**, 507–514.

Skarzynski, T. (2013). *Acta Cryst.* D**69**, 1283–1288.

Śledź, P., Kamiński, R., Chruszcz, M., Zimmerman, M. D., Minor, W. & Woźniak, K. (2010). *Acta Cryst.* B**66**, 482–492.

Sørensen, H. O. & Larsen, S. (2003). *J. Appl. Cryst.* **36**, 931–939.

Stash, A. & Tsirelson, V. (2002). *J. Appl. Cryst.* **35**, 371–373.

Stash, A. I. & Tsirelson, V. G. (2005). *Crystallogr. Rep.* **50**, 177–184.

Stevens, E. D. & Coppens, P. (1980). *Acta Cryst.* B**36**, 1864–1876.

Volkov, A., Li, X., Koritsanszky, T. & Coppens, P. (2004). *J. Phys. Chem. A*, **108**, 4283–4300.

Yagi, N., Inoue, K. & Oka, T. (2004). *J. Synchrotron Rad.* **11**, 456–461.

Zarychta, B., Zaleski, J., Kyzioł, J., Daszkiewicz, Z. & Jelsch, C. (2011). *Acta Cryst.* B**67**, 250–262.

Zhurov, V. V., Zhurova, E. A., Chen, Y.-S. & Pinkerton, A. A. (2005). *J. Appl. Cryst.* **38**, 827–829.

Zhurov, V. V., Zhurova, E. A., Stash, A. I. & Pinkerton, A. A. (2011). *Acta Cryst.* A**67**, 160–173.

electronic reprint